CSC Report 93-34

A Large Motion Zero-Gravity Suspension System for Experimental Simulation of Orbital Construction and Deployment

Timothy Milton Straube

CENTER FOR Space Construction
University of Colorado
Campus Box 529
Boulder, CO 80309-0529
(303) 492-4960

A Large Motion Zero-Gravity Suspension System for Experimental Simulation of Orbital Construction and Deployment

Timothy Milton Straube

Thesis, Master of Science
Department of Aerospace Engineering Sciences
December 1993

Center for Space Construction
University of Colorado, Boulder

A NASA University Space Engineering Research Center
Funded by NASA Grant NAGW-1388

Straube, Timothy Milton (Masters of Science, Aerospace Engineering Sciences)

A Large Motion Zero-Gravity Suspension System for Experimental Simulation of Orbital Construction and Deployment

Thesis Committee: Chairman, Professor Lee D. Peterson

Professor K.C. Park

Professor Martin M. Mikulas

ABSTRACT

This thesis describes the design and implementation of a vertical degree of freedom suspension system which provides a constant force off-load condition to counter gravity over large displacements. By accommodating motions up to one meter for structures weighing up to 100 pounds, the system is useful for experiments which simulate orbital construction events such as docking, multiple component assembly, or structural deployment. A unique aspect of this device is the combination of a large stroke passive off-load device augmented by electromotive torque actuated force feedback. The active force feedback has the effect of reducing break-away friction by a factor of twenty over the passive system alone. The thesis describes the development of the suspension hardware and the control algorithm. Experiments were performed to verify the suspensions system's effectiveness in providing a gravity off-load and simulating the motion of a structure in orbit. Additionally, a three dimensional system concept is presented as an extension of the one dimensional suspension system which was implemented.

ACKNOWLEDGMENTS

This work was supported by NASA Headquarters Grant NAGW-1388 through the Center for Space Construction at the University of Colorado, and by NASA Langley research center grant NAG-1-1490 through the Center for Aerospace Structures with Dr. Harold Bush as technical monitor. The project used the facilities of the McDonnell-Douglas Aerospace Structural Dynamics and Control Laboratory at the University of Colorado. Special recognition should go to undergraduates Mr. Robert "Kipp" Shearman and Mr. Andy Wobido who assisted in the research and development, and who also performed the experiments for the three dimensional system. I also wish to thank Mr. Walter Lund and Mr. Jim Kastengren, who oversaw development of the electrical and mechanical systems. And finally, I would like to acknowledge the control system development efforts of Mr. Steve Kranock and Mr. David Smart.

TABLE OF CONTENTS

LIST OF TABLES

LIST OF FIGURES

1.0 INTRODUCTION

1.1 Purpose and Rationale

Orbital missions are always preceded by ground testing to validate the mechanics of spacecraft structures and produce an improved prediction of its orbital response. A variety of devices and apparatus are used to model some aspect of the orbital environment so as to improve the accuracy of the ground test. These simulations often model orbital temperature, radiation, vacuum level, and gravity. This research focuses on a new method for simulating orbital gravity effects on a structure. Experimentally, this is accomplished by producing a constant force gravity off-load using a mechanical suspension system in a 1-g laboratory.

To simulate the zero-gravity, unrestrained motion of a structure, a suspension system must exactly support the weight of the structure throughout the entire region of motion while introducing no extraneous constraint forces on the test article. Generically, a suspension system is composed of five components [Figure 1]. Acting together they provide the off-load of the test article's weight and allow for test article motion.

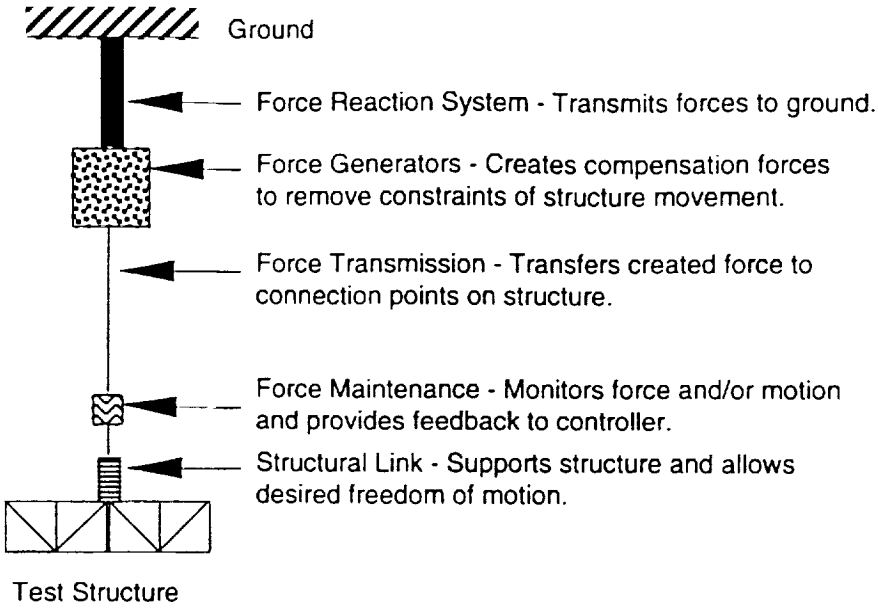

Figure 1. General suspension system components

Many existing devices are capable of constantly off-loading a structure's weight over various ranges of motion. None exactly meet the long range goals of this research: a suspension system which will allow terrestrial simulations of spacecraft docking, deployment, or assembly. The required suspension system must allow for three dimensional motions up to 1 meter and test articles weighing up to 100 pounds. This thesis will focus on the creation and verification of the first generation hardware, support equipment, and controller of a one-dimensional Degree Of Freedom (DOF) suspension system which has a three dimensional extension.

Like all suspension systems, the device implemented in this research off-loads gravity by applying a nearly constant force at a finite number of test article connections. This limitation means that the test article will still undergo sagging and internal stresses due to its own weight. In this way, true micro-gravity is not simulated. In a rigid body sense however, the response can closely match that of an orbiting structure. Some possible experimental uses of such a suspension system are shown in figure 2.

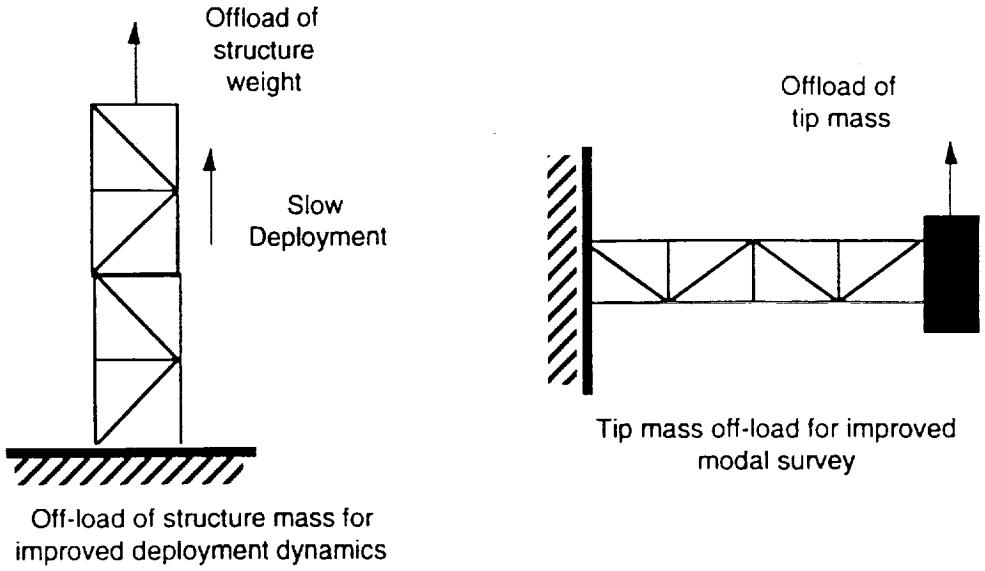

Figure 2. Suspension system experimental uses

1.2 Techniques for Off-loading Test Article Weight

A number of methods and devices have been used to simulate microgravity dynamics by countering the test article weight. The projected uses of this particular suspension system suggest a design with long stroke capabilities and three dimensional motion. The following sections describe a number of approaches that have been used in the past.

Free Fall Techniques

It is possible to achieve microgravity for short periods of time in aircraft flying parabolic trajectories. This environment is limited to tests no more than 25 to 30 seconds long, so that they are unsuitable for the study of spacecraft orbital construction, whose experiments are generally much longer. The expense of this approach is prohibitive for routine application.

Long Cables

A structure suspended from very long cables is generally free from constraining forces in the horizontal direction over significant distances. Besides the inability to provide a vertical DOF most facilities cannot provide the overhead clearance to create near zero pendulum restoring force. In many experimental structures laboratories very soft cables or springs are used as the support mechanism during modal surveys.

Counterweights

A counterweight is one of the most simplistic methods of off-loading a structure with a constant force. This approach results in a mass loading of the system which must be accounted for when examining any results.

Air Bearings

These systems allow virtually frictionless movement in the horizontal plane over very large distances. The primary limitation is the lack of vertical and rotational degrees of freedom. Spherical air bearings also exist which provide rotational degrees of freedom through limited, approximately 20° [1], angular displacements. Spherical air bearings coupled with an air bearing surface provide five degrees of freedom.

Pneumatic Devices

When supported on an air lubricated piston, a test article experiences an almost zero stiffness from the suspension device [1,2]. Current designs have demonstrated a stroke of 18 inches. Disadvantages include the high cost and complexity of the system. Additionally, the concept also has limitations when extended to three dimensions. Pneumatic off-loads provide only a constant force. Many three DOF configurations require the off-load to change with test article position.

Springs and Zero Spring Rate Mechanisms

Very long, low stiffness springs exhibit only small changes in force over significant distances. A test article may translate through this region in approximate zero gravity off-load conditions. A useful effective range requires extremely long spring deformation to provide the support force. Torsional springs can relieve problems due to overhead clearance. Theoretically a torsion spring can be made with low enough stiffness to satisfy any desired criteria. As a practical matter, limitations in spring size and fabrication do exist.

Many types of Zero Spring Rate Mechanisms (ZSRM) use combinations of springs and mechanical levers to provide very close to zero to stiffness. Most mechanisms found in the literature search, however, exhibit a range of motion of two to four inches [3, 4, 5]. One device, utilizing a torsional spring and non-circular disk, was found which theoretically has zero stiffness over large regions [6, 7].

Active Force Feedback

Active feedback of the suspension systems supporting force can allow a simple motor or actuator to provide the required off-load [8]. For large structural weights, such a system requires very large actuators to off-load test article weight. A brief comparison of motors shows that high torque high precision motors are very expensive. These systems can also pose a possible safety hazard if the active system, which is the only test article support, unexpectedly shuts down.

1.3 System Requirements

This section reviews requirements on the suspension system design which are necessary to ensure an accurate representation of the structures mechanics. Most of these requirements are derived from experiences in the literature.

Effects of Parasitic Mass, Stiffness, and Damping

An accurate microgravity simulation requires that a test article's suspended response match, as closely as possible, its zero-gravity dynamics. This requires that the added mechanics of the suspension system must be minimized. Consider first the effect of the suspension system mass. The suspension system's moving mass should be kept to a minimum to lesson the effect on the structure's rigid body modes. This mass directly effects the structure's Newtonian dynamics by adding additional mass ΔM, to the system. From

$$F = (M + \Delta M) \times a$$

it is obvious that this mass has the effect of reducing the structure's acceleration, a, for any given imparted force, F. An acceleration within 5 to 10% of the expected acceleration was established as a reasonable goal for the first generation design. This criteria corresponds to a suspension system mass which is 5-10% of the test article mass. This is similar to the target suspension mass set forth in research for a suspension system designed at Phillips Laboratory [1].

It is also important that the vibration frequencies of the suspension system be well separated from the fundamental modes of the structure. Failure to achieve this requirement may cause modal coupling between the structure and the suspension system, which can cause a frequency shift or change in the mode shapes of the structure. Prior work indicates that suspension modes should be no greater than one-fifth of the supported structures fundamental mode [1, 2, 3].

System friction can also limit the fidelity of the zero-gravity simulation. In fact, the study done by the Phillips Laboratory [1] states that friction was a main source of the errors that they observed. System friction inhibits performance in two ways. Friction

will increases the damping in some modes of the suspended structure, but it also will reduce rigid body acceleration and deployment by counteracting some of the input forces.

Experimental System Requirements

The baseline system requirements were chosen to accommodate a variety of possible uses. These requisites were developed based on the suspension system's anticipated use in space construction related experiments, including slow deployment, rigid body slewing, and multiple component assembly. These requirements lead to specifications in displacement and load capacity.

Displacements were required to be as large as one meter. This necessity eliminated a number of possible off-load methods from consideration. The pneumatic devices and most ZSRM do not exhibit the necessary stroke. Air bearing surfaces and long cables do not provide the necessary freedom in the vertical direction.

The system load capacity should range from 10 to 100 lbm. The baseline structure for the design was chosen to be an eight bay Warren truss weighing 38.9 lbm with a fundamental frequency near 50 Hz. This leads to a fundamental suspension frequency less than 10 Hz, and system inertial mass on the order of 1 to 5 lbm. For 100 lbm structures, active off-loading becomes impractical because of the size of motor that would be necessary.

Finally, as mentioned earlier, the configuration should provide three dimensional motion or at least provide a technological step towards a system with three dimensional capabilities.

1.4 Design Approach

After a review of the literature and the system requirements, a design utilizing a large motion ZSRM with active compensation was selected. This combination of a passive with active force feedback controller combines the advantages of both systems.

Active systems, such as pneumatics or servo motors, have an advantage over passive systems because feedback allows the user to have precise control over performance of the system. In some instances, these systems also avoid the large mass and friction associated with mechanical systems. They are in general very expensive to develop and maintain, especially as the off-load weight requirement gets larger.

In contrast, the cost of a passive system is less, especially for large off-load weights. Passive systems are also immune to failure in electrical equipment such as computers or the load-bearing actuator which may be a safety concern if power shuts down unexpectedly. By combining the passive and active system, the passive system will provide the nominal off-load, and the active system will minimize the effects of mechanical imperfections.

The final configuration developed in this research consists of a large stroke passive off-load mechanism augmented with electromotive force control via a DC servo motor [Figure 3]. The configuration is similar to a design implemented in a Phillips Laboratory experiment [1], except that the design utilizes a mechanism with constant off-load force throughout a large range of motion. In addition, this concept includes a load cell at the test article connection which provides the feedback element for the controller. While the passive off-load completely supports the test article weight, the active force feedback improves system response by compensating for friction and suspension mass. Inherently stable, the passive off-load provides a safeguard against electrical failures and also reduces the actuator size requirements, a factor which reduces the system's overall cost.

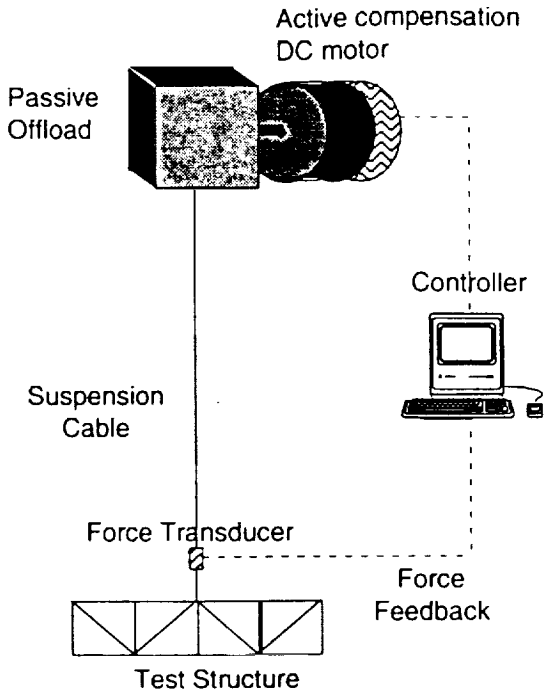

Figure 3. Passive-plus-active concept implemented in research

1.5 Thesis Organization

Section 2.0 of the paper describes the implementation of the passive-plus-active suspension system. This includes details off the passive off-load scheme and the feedback control loop. Section 3.0 describes tests performed with rigid body test articles to optimize the feedback control scheme and evaluate the zero gravity simulation characteristics of the suspension system. Section 4.0 examines the suspension system's effect on the modal characteristics of a suspended structure. Section 5.0 looks at a three dimensional system utilizing the concepts developed for the single DOF configuration. Finally, section 6.0 makes conclusions about the effectiveness of the suspension system and discusses possible improvements for second generation implementation.

2.0 SYSTEM IMPLEMENTATION

The two distinct subsystems, the passive off-load and the active feed back loop, work together to produce the best system performance. The design methodology and rationale are specified in the following sections.

2.1 Passive Sub-System Design

The Large Stroke ZSRM concept

The passive subsystem, a ZSRM capable of large ranges of motion, consists of a torsion spring and a non-circular disk [Figure 4]. The test structure is supported by a cable which wraps around the disk after passing across overhead pulleys and through the cable guide [Figure 5].

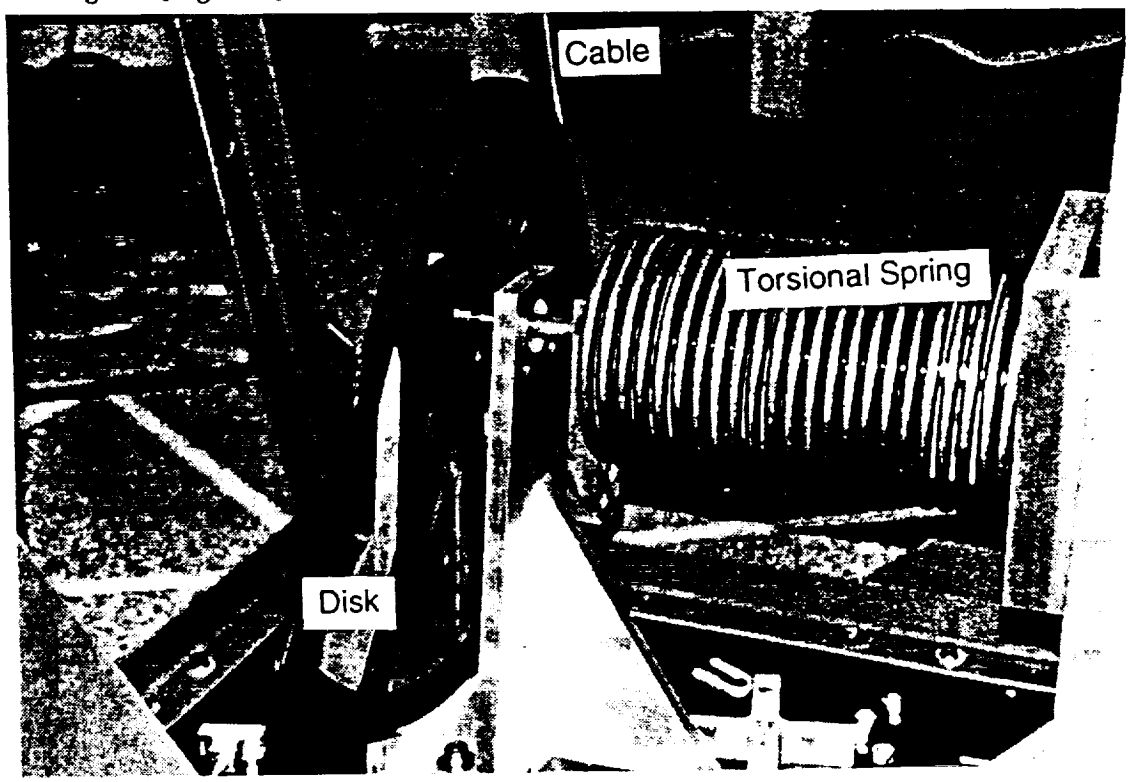

Figure 4. Photo of the large stroke ZSRM

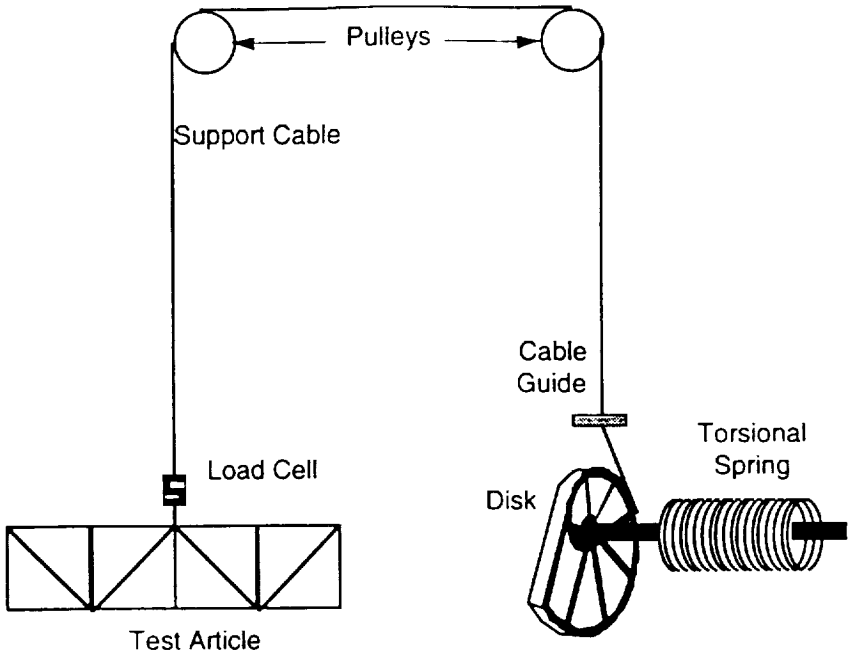

Figure 5. Linkage to the test article

Given an initial rotation, β_0, the torsional spring produces a torque, M_{spring} on the disk given by,

$$M_{spring} = (\beta_0 + \theta) \times K_s,$$

where θ is disk rotation and K_s is the spring rate. This is offset by the equal magnitude moment created by the cable force around the center of the disk,

$$M_{cable} = W \times D(\theta).$$

$D(\theta)$ is the perpendicular distance from the cable to the center of the disk and W is the weight of the test article. It should be noted that this distance is not the same as the radius of the disk $R(\theta)$, at the tangent point of the cable on the disk. Figure 6 shows the locations of these parameters. Assuming that the cable force W is independent of θ, equilibrium establishes a relationship between the rotation angle of the disk, θ, and the required moment arm of the disk at that rotation, $D(\theta)$:

$$(\beta_0 + \theta) \times K_s = W \times D(\theta)$$

As the disk rotates, the effective moment arm, $D(\theta)$, of the cable force changes such that the torque from the torsion spring is balanced.

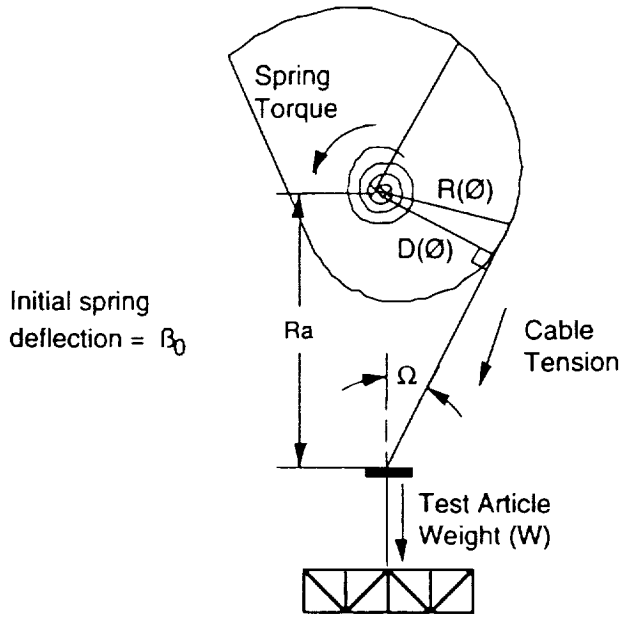

Figure 6. Spring torque balanced by the test article weight

Disk design

The equations for this type of zero spring rate mechanism were developed in a paper by L.F. Yang [6]. The concept is also referred to in a book on classical mechanisms by N.P. Chironis [7]. Yang's equations for the disk profile were used to determine the coordinates of the disk shape. From the equations which define the disk profile, five independent parameters completely specify the entire passive system configuration given a specific test structure weight, W: K_s is the spring rate of the torsion spring, β_0 is the initial deflection of the spring, θ_{up} and θ_{down} are the furthest rotation of the disk from the nominal position, and Ra is the distance from the center of the disk to a "stationary cable guide" [Figure 7]. The disk profile is such that a test article of any weight can be supported provided a new torsion spring is used to maintain the parameter, $\alpha = W / K_s$. Current configurations were designed for W = 38.9 lbm, the weight of the baseline test article.

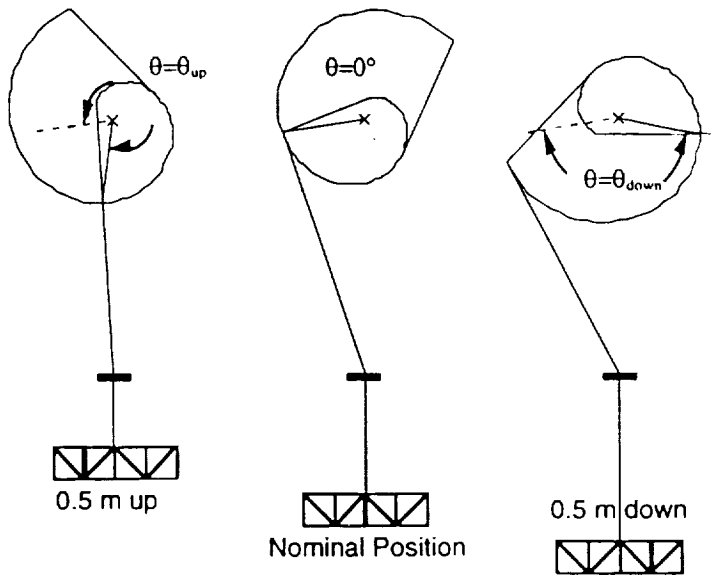

Figure 7. Disk rotation and corresponding test article translation

The disk design was optimized to take into account a number of considerations while maintaining the primary requirements for translation in excess of 1 m. Disk size was determined by a number of factors. A small disk gives the cable force a smaller moment arm which creates a smaller torque on the disk. This reduces the size of the torsional spring and the servo motor that are necessary, which brings down system costs.

To maintain the range requirements with a smaller disk requires a greater disk rotation. The rotation limit is fixed by two things. For a single plane disk, the total rotation angle is constrained to less than 360° . To remove this restriction, the design uses a conical helix shaped disk grove which will allow any amount of rotation and still maintain a convex groove shape. While adding complexity and manufacturing costs, this design allows for greater rotation and corresponding test article translation.

Another limitation to rotation angle is the torsional spring. A spring undergoing large rotations approaches its stress limits and the end of its linear range for restoring torque. To reduce the potential size of the spring, a 540° maximum rotation limit was

set. To reduce the number of spring coils and average coil diameter, the spring rate, K_s, was limited to 5.0 Nm/rad.

Another important consideration was the friction between the cable and the cable guide. The cable produces a side load, F_{sl}, on the cable guide equal to:

$$F_{sl} = 2 \times W \times \sin(\frac{\Omega}{2}),$$

where Ω, is the cable incidence angle [Figure 7]. Because the friction force is proportional to the loading force, the angle Ω needs to be kept as small as is practical. The angle can be reduced by moving the cable guide further from the disk center, but this forces the system housing to be larger in order to support the cable guide. The disk size can also be reduced to lessen the angle so long as the other requirements are satisfied. A number of designs which met the guidelines were considered. Table 1 summarizes the selected disk parameters.

Table 1. Disk design parameters

Initial spring deflection	$\beta_0 = 360°$
Maximum angular rotation up	$\theta_{up} = 290°$
Test article translation up	0.52 m
Maximum angular rotation down	$\theta_{down} = 160°$
Test article translation down	0.56 m
Distance from disk center to cable guide	$R_a = 0.165$ m
Frequency parameter	$\alpha = 1.907$ rad/m
Maximum disk radius	0.2394 m
Minimum disk radius	0.04227 m
Cable guide incident angle	$\Omega = 27.9°$
Final design weight	1.5 pounds

The disk itself was machined from a single 3/8" aluminum tooling plate. One of the machine drawings for the disk is shown in figure 8.

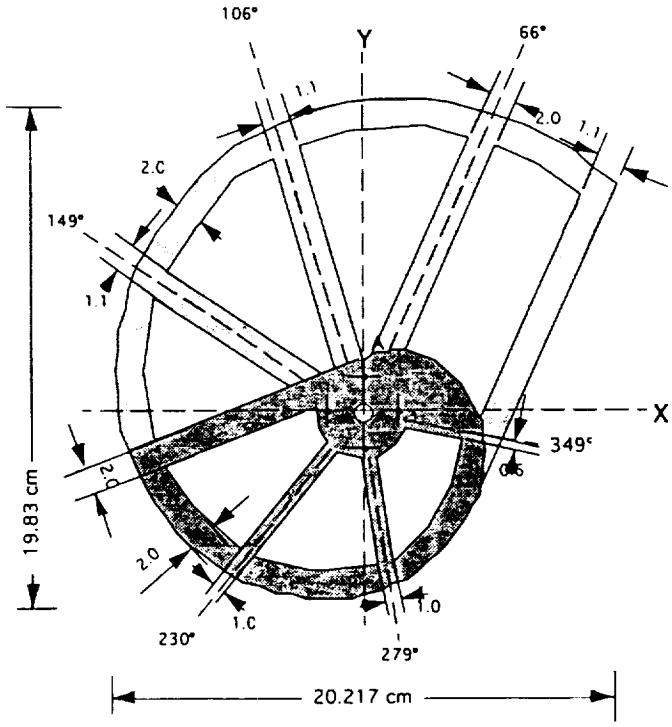

Figure 8. Machine drawing of the disk

Spring/Mandrel Design

The next step was the selection of the torsional spring. The disk shape dictated a spring rate of K_s = 4.5 Nm/rad, for the 38.9 lbm test article. This also established the system parameter, alpha = 38.18 rad/m, the initial spring rotation, β_0, and the springs rotational range θ_{up} and θ_{down}. Since the spring's maximum rotation is given by,

$$\theta_{\max} = \beta_0 + \theta_{down} = 520°,$$

the maximum restoring force from the spring is:

$$T_{\max} = \theta_{\max} \times K_s = 40.84 Nm$$

From these parameters, the final spring design [Figure 9], was established following the methodology in "Newcomb's Spring Design Manual" [9]. Table 2 summarizes the spring design.

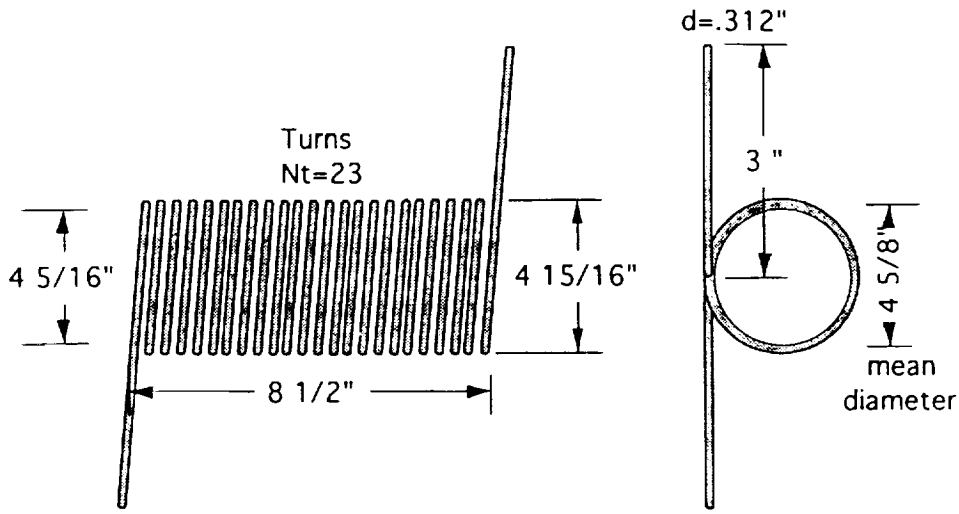

Figure 9 Torsional spring design drawing

Table 2. Spring design requirements

Torque Requirements	
Spring constant	4.5 Nm/rad
Maximum deflection	1.44 turns = 520°
Maximum torque	40.8 Nm
Wire Requirements	
Type	Oil Tempered
Wire diameter	0.312"
Maximum stress	174 kpsi
Design stress	121 kpsi (70% max)
Modulus elasticity	30 Mpsi
Spring Design	
Mean diameter	4 5/8"
Number of coils	23 ± 15°
Free length	8 1/4" ± 1/8
Working range	70° to 520°

An additional issue was inter-coil friction during extreme deflection. As the spring deflects, the coils move closer together. Eventually they touch, creating friction. The

coil pitch was designed to provide coil separation such that a gap will remain between all the coils at the highest torque level.

Spring sag and friction against the supporting mandrel were not as easily addressed. Sagging, caused by the springs weight, can cause unpredictable spring torque or buckling under extreme load. Initially, a solid mandrel [Figure 10] was placed inside the spring for support. The mandrel was free to rotate on the shaft. Upon rotation the spring deflects laterally, causing binding between the spring and the mandrel. As the disk rotates only one end of the spring rotates, the other remains fixed to the housing. When the mandrel binds at one end of the spring, friction is created between the mandrel and the parts of the spring rotating at a different rate. To alleviate this problem two steps were taken. First, a new mandrel consisting of a number of one inch pieces [Figure 10] replaced the existing full length mandrel. This allowed the mandrel pieces to rotate with the portion of the spring that it supported, minimizing any rotational differences. Second, the entire spring and mandrel pieces were coated with Xylon [10], a friction reducing treatment.

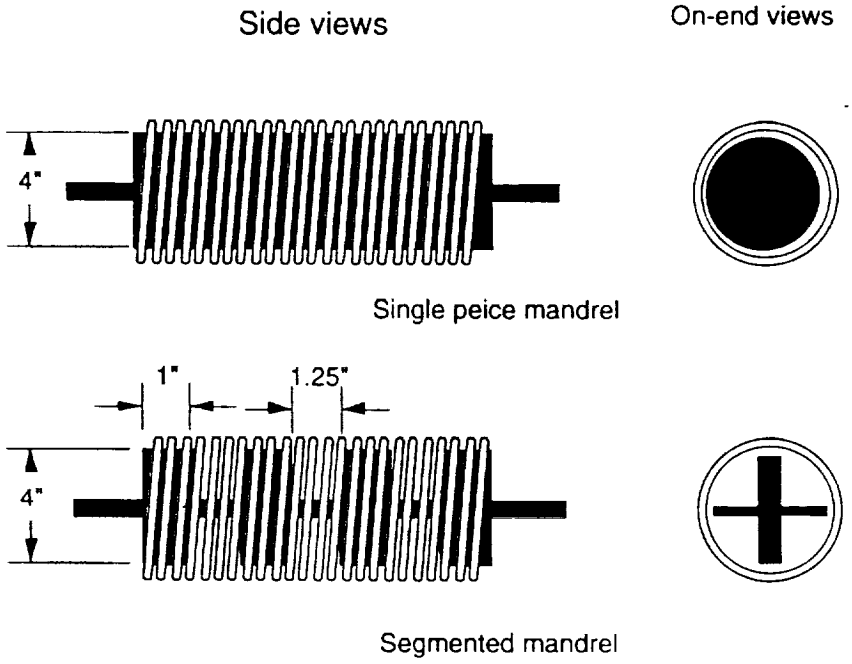

Figure 10. Solid and piecewise mandrel designs

Test Article Link

The disk is mounted to a shaft which is directly linked to the drive shaft of the motor. The same shaft supports the spring mandrel. All of this hardware, as well as the wire guide, is supported by a housing [Figure 11] which is hard mounted to the floor. A 1/16" aircraft cable starts from the disk and passes over a small low friction bearing which act as a cable guide. The cable then passes through two overhead pulleys affixed to the ceiling and down to the fixture point on the test structure. This configuration [Figure 12] was chosen because the floor mounted off-load provides easy access to all components during initial testing. Many other configurations are possible since the passive system is designed as a self-contained unit. Other possible arrangements could include placing the system in an inverted position or horizontally cantilevered [Figure 13].

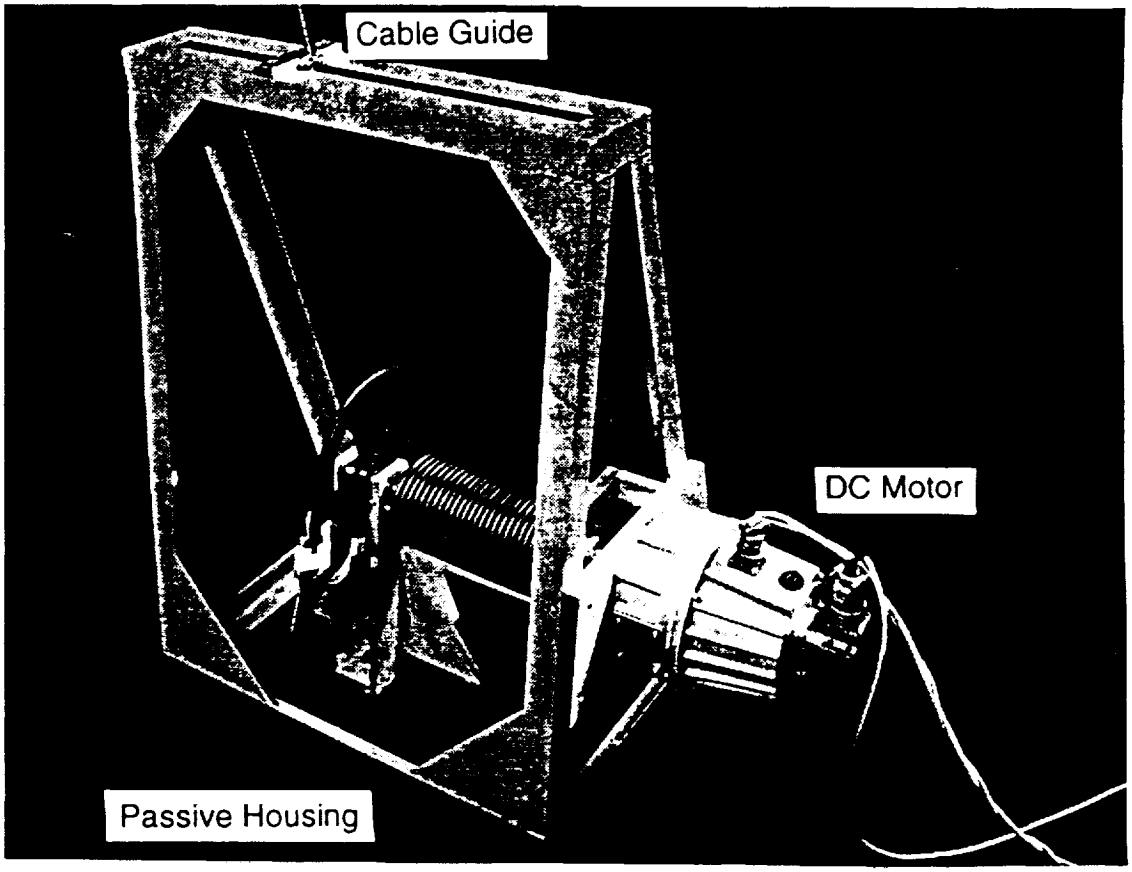

Figure 11. Photo of the passive off-load system in its housing

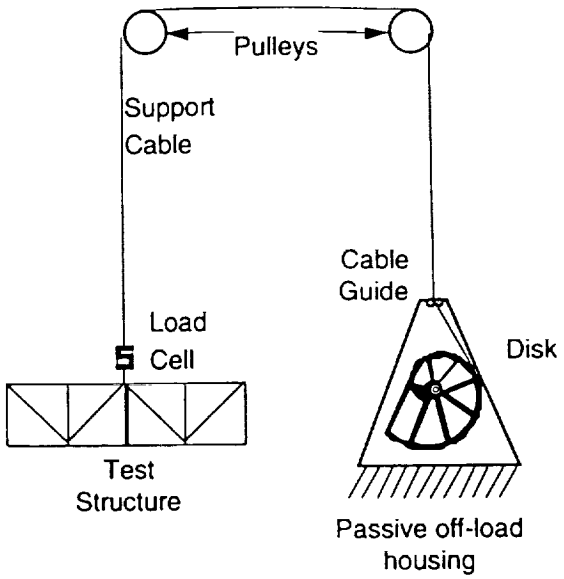

Figure 12. Implemented passive system configuration

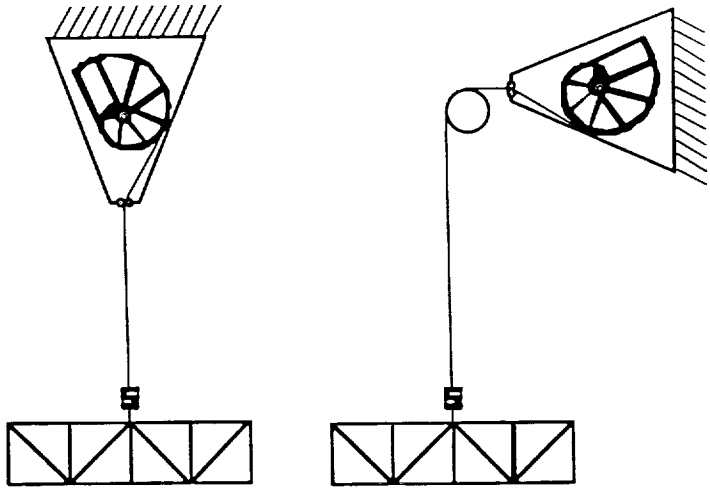

Figure 13. Other possible passive system configurations

2.2 Active System

The active system [Figure 14] is driven by feedback from a load cell in the cable path near the test article. Accurate gravity off-loading requires that the cable tension equal the weight of the structure. Any input force on the test article will cause the cable tension to deviate from this value. The controller reacts to the error signal and commands the servo motor to respond such that the acceleration of the test article

returns the cable tension to the test article weight. In this way, the active system compensates for the imperfections in the passive system.

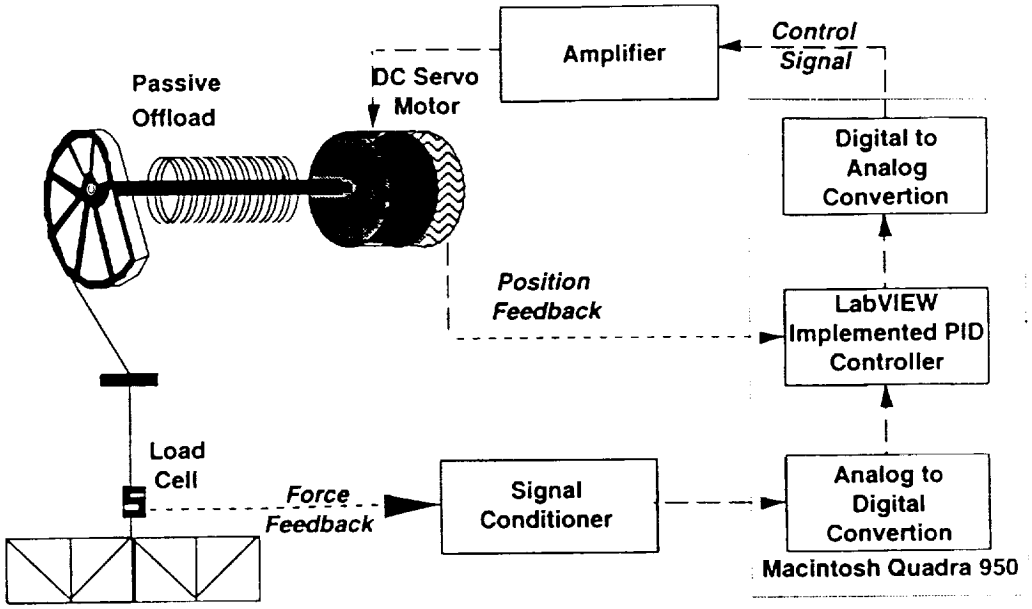

Figure 14. Controller hardware diagram

Actuator Motor Selection

Control actuation is achieved via a brushed DC servo motor and servo amplifier which were chosen to fulfill a number of requirements. The controller adjusts the motor torque to command cable tension and consequently the load cell reading. The motor size was based on the tolerance of the spring torque rate which was given as ±5% by the spring manufacturers. This meant that at any rotational position it was possible the spring would be 5% under expected torque values, thus forcing the motor to off-load 5% of the weight of a test article. For a maximum test article weight of Wmax = 100 lbm. at the maximum radius of the disk R_{max} = 0.238 m the resulting motor torque becomes:

$$T_{max} = 5\% \times 0.239m \times 100lbf = 750oz \cdot in$$

Other important consideration were motor friction, both static and kinetic, inertia and ability to provide smooth torque, usually measured as clogging and ripple. The ability to add an encoder to measure test structure position was also a requirement.

In a DC motor the torque is governed by the current in its windings and the strength of its magnet. This requires an amplifier with a current control mode so that the controller has direct command authority over motor torque and consequently cable tension. It was also desirable for the amplifier to have an internal current monitoring loop, which insures proper current, to alleviate the need for an external control loop.

The amplifier needs to provide the peak and continuous current needs of the motor. Amplifier linearity and noise considerations were also important. An Advanced Motion Controls 30A-AC switching amplifier was chosen. The current to the motor was controlled by applying a voltage to the amplifiers input. An input of ±10 volts to the amplifier corresponds to the amplifier's maximum range of ±30 amps output. This was the amplifier's peak current value, which could only be held for short periods of time, 1 to 2 seconds, at which time the current decays to the maximum continuous value, 15 amps, which can be maintained indefinitely. The final characteristics for the motor and amplifier chosen are shown in Table 3.

Table 3. Motor characteristics

Manufacturer	PMI Motion Technologies
Motor type	JR16M4CH-1
Motor Characteristics	
Peak torque	5374 oz•in
Stall torque	510 oz•in
Peak current	79.0 amps
Continuous stall current	7.64 amps
Clogging torque	0 oz•in
Friction torque	11.0 oz•in
Moment of inertia	0.075 oz•in sec•sec
Encoder Characteristics	
Moment of inertia	0.0003 oz•in sec^2
Starting friction	1.0 oz•in

Table 4. Servo amplifier characteristics

Manufacturer	Advanced Motion Solutions
Type	30A20AC
Peak current	30 amps
Maximum continuous current	15 amps
Switching frequency	33 kHz
Bandwidth	2.5 kHz

Controller

The control logic for the system was implemented in LabVIEW [11]. Before the control loop is executed a number of initialization steps occur. The analog-to-digital and digital-to-analog hardware as well as the signal conditioning equipment are initialized to accept data. A load cell reading is also take to be used as a standard value to be compared with subsequent readings.

After initialization is completed the control loop [Figure 15],is executed at 150 Hz until the user manually terminates the controller or the test article translates beyond the preset bounds established by the user. In the first step of the control loop the most recent data from the load cell is read into memory from the 16 bit analog to digital converter. This voltage is converted to a force and compared to the load cell reading from the experiment initialization. Before the signal reaches the integrator it is processed by a voltage dead band which zeros any signal whose absolute value is below a user defined level. Any error greater than the dead band level is not effected.

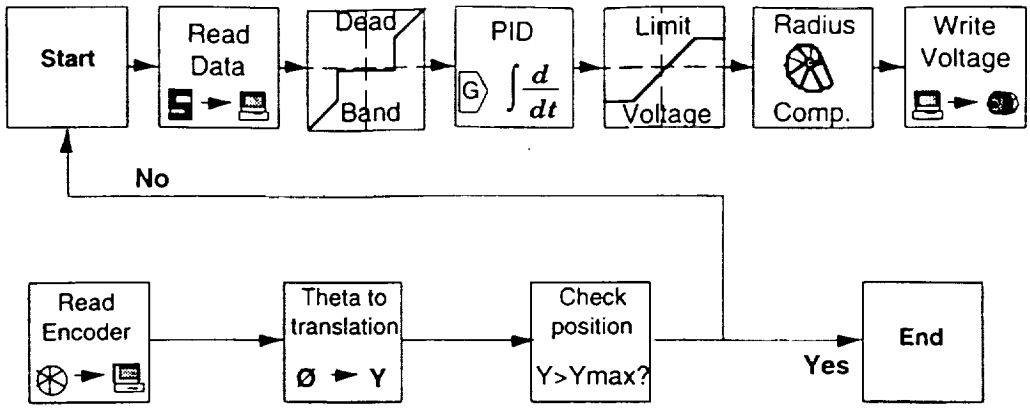

Figure 15. Control logic diagram

The error, now in pounds, enters the Proportional, Integral, Derivative (PID) logic block. Its voltage output is based on a proportional, integral, or derivative relationship with the load cell error. The exact formulation follows:

$$VoltageOut = K_p X(n) + K_d \frac{X(n) - X(n-1)}{\Delta T} + K_I \sum_{k=1}^{k=n} \frac{X(k) + X(k-1)}{2} \Delta T,$$

where $X(n)$, is the load cell error at each discrete time step, ΔT, after processing by the dead band. K_p, K_d, and K_I, are the proportional, derivative and integral gains. Anyone type of control, proportional, derivative, or integral, can be used by setting the gain for the other two to zero. The voltage from the PID passes through a safety limit before being processed by the disk radius compensation.

Because of the disk's shape, a motor torque will have a different effect depending on the rotation angle. A torque exerted at a large disk radius will result is a smaller change in cable tension than a torque exerted at a smaller disk radius. This condition may cause the controller to behave inconsistently as the test article translates and the effective moment on the disk becomes larger or smaller. The radius compensation scales the voltage sent to the amplifier so that the effective force on the cable is the same for all disk orientations. Finally, the control voltage is added to the constant DC holding voltage and sent to the 12 bit digital to analog converter and out to the amplifier.

The control loop also includes sampling of a digital signal from the encoder. The angular rotation is converted to an estimate of the test article position. Should the test article leave the test zone the controller automatically shuts down. All experimental results presented in the paper include the values of the dead band and PID gains used.

System Sensors and Signal Conditioning

Control feedback is achieved through a load cell which links the cable and the test article . This load cell must be able to quickly respond to any changes in cable tension and also endure the wide range of loads from different test articles. Table 5 lists the characteristics of the load cell.

Table 5. Load cell characteristics

Manufacturer	Sensotec
Type	Model 81 strain gage
Load capacity	100 lbf
Hysteresis	0.03 lbf
Non-repeatability	0.02 lbf
Output	0.05 volts/lbf

An in-line bi-polar amplifier powers the load cell and provides amplification to the output signal. After zeroing the amplifier prior to each test, the final transducer sensitivity is 4.9975 volts out of the amplifier per 100 lbf. tension applied to the load cell.

After leaving the bi-polar amplifier the signal is processed by a anti-aliasing low pass filter and gain stage before digitization. The Frequency Device 9064 uses a low-pass eight pole butterworth filter which was set to a 30 Hz cutoff frequency as determined by the 150 Hz sampling rate and the resolution of the digitizer.

In addition to measuring cable force, the position of the test article was monitored via an encoder on the DC motor. The encoder sends out a digital pulse each time it rotates a

an incremental angle. The encoder used in the experiment has 4000 increments per revolution or a resolution of 0.09 degrees. These pulses are counted by a computer board and then converted back to the angle of the motor. From the rotational angle and disk shape, an approximate relation was found between the angle of rotation and the test article translation, y, as follows:

$$y = -3.88 \times 10^{-6} - 6\theta^2 + 0.0029\theta .$$

Empirical results showed that this measurement was reliable to a resolution of approximately 0.002 m.

The position data derived from the encoder was used not only as a safety device but also as an experimental verification. To ensure system controllability the control loop included a read of the encoder and determination of the test article position. If the test article position exceeded the preset bounds, the controller terminated function. This proved very useful while tuning the controller because at times the gains chosen caused the system to go unstable. Additionally, the test article position information was used as a parameter to verify performance during rigid body acceleration tests. The derivatives of the position data provided estimates of test article velocity and acceleration.

3.0 RIGID BODY EXPERIMENTATION

Once the passive-plus-active suspension system was implemented, a number of tests were performed to determine its effectiveness in off-loading gravity for rigid body elements. Initial tests determined the best controller configuration and then free-free simulations were performed with various levels and types of input forces.

3.1 Test Articles

All of the rigid body tests were performed using a lumped mass test article. This ensured that any observed low frequency modes were from the suspension system. For the passive-plus-active system a 38.9 lbm solid steel cylinder 5.5 inches in diameter and 5.75 inches tall was used. An eyebolt was tapped into one end to provide an attachment to a hook which extended from the bottom of the load cell [Figure 16].

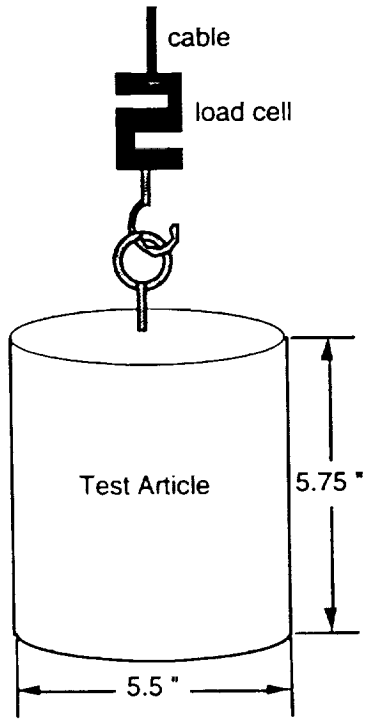

Figure 16. Passive-plus-active test article

3.2 Input Force Types

For tests performed with the lumped mass, real and virtual forces were used. Virtual forces provided a consistent and expeditious method for evaluating and configuring the controller, while the real loads demonstrate the suspension systems capability for simulating microgravity under experimental conditions. Two types of force histories were applied during testing; impulse and constant force tests. A constant force test applies a load for the entire duration of the test to produce a constant test article acceleration. During impulse testing the load was applied for a short duration to produce a constant velocity. These are further explained in the following sections.

Virtual Force Tests

To impart a virtual force, an offset is added to the load cell voltage, creating an error signal inside the control loop. This error is processed by the controller which instructs the amplifier and motor to respond as if an ideal force has acted upon the test article. The result is a constant acceleration.

Virtual testing provided a repeatable force, which maintained consistent magnitude and duration over may experiments. Systematic tests were performed with various controller configuration utilizing a constant virtual force. Subsequently any changes in system performance were directly attributable to variations in the control parameters. With these results, the best controller for a specific criterion can be chosen.

Real Force Tests

Tests performed with real forces provided an evaluation of the system's performance in matching theoretical accelerations. Constant force tests were performed by initializing the controller with the base test article weight and then, with the controller on, placing

additional mass on the test article. The additional weight creates a downward acceleration of the test article.

This type of testing is sensitive to errors in measuring the imparted force. The impact dynamics of placing and removing a mass from the system contained a transient which could not be determined and probably also included random input forces by the experimenter. Although the net input force of these inputs is small, they also have an effect through the moments they induce. Any off-center forces create a moment which tends to cause the test article to swing, exciting some of the suspension modes.

3.3 Controller Tuning

A number of tests were necessary to optimize the PID control gains and the load cell error dead band level to produce the best simulation of free-free boundary conditions.

Controller Gains

Experiments were performed to determine if each type of feedback; proportional, integral, and derivative, could track a constant input force and produce a constant acceleration with the correct magnitude. After trial and error with all three types of gains at various levels it was determined that only a pure integral gain could accurately compensate for the friction in the passive system and produce the correct acceleration. The difficulties with the proportional and derivative gains are described below.

Because of friction inherent in the passive system the motor must produce some torque to offset the friction force. As an external force is applied to the test article, a load cell error appears. In the case of a proportional controller, if the gain is not large enough to overcome the system friction, no motion occurs. At some level of gain, the friction is overcome and the test article is set into motion. Once the test article reaches the appropriate acceleration the load cell error drops to zero, and so does the controller

output. At this point, the motor is applying no torque to overcome friction. Friction slows and stops the test article and the load cell error rises again. The continuing cycle drives the system into an oscillation.

A different problem occurs with the derivative gain. It can only respond to a change in the load cell reading. Again, if the gain value is small the test article will not move, friction is not overcome, and a constant load cell error will appear. The derivative gain can not respond to a constant error, only changes in error. If the gain is large friction is overcome, the test article will start in motion, and the load cell error will go to zero. The derivative gain responds to the drop in load cell error with a force in the opposite direction. Again an oscillation is established which may or may not go unstable.

Both of these effects were observed in experimental tests. These tests showed that, by themselves, proportional and derivative gain cannot compensate for the system friction. Integration gain is the only usable option.

Figure 17 shows a typical response to a constant force with integration gain only. At time 0, the input force attempts to accelerate the test article but is hindered by system friction and inaccuracies in the passive off-load. Because the test article is not accelerating at the appropriate magnitude a load cell error signal develops, which is integrated by the controller, from 0 to .50 seconds on figure 17. At .50 seconds the controller output level is such that output torque from the actuator corrects the acceleration and the load cell error goes to zero.

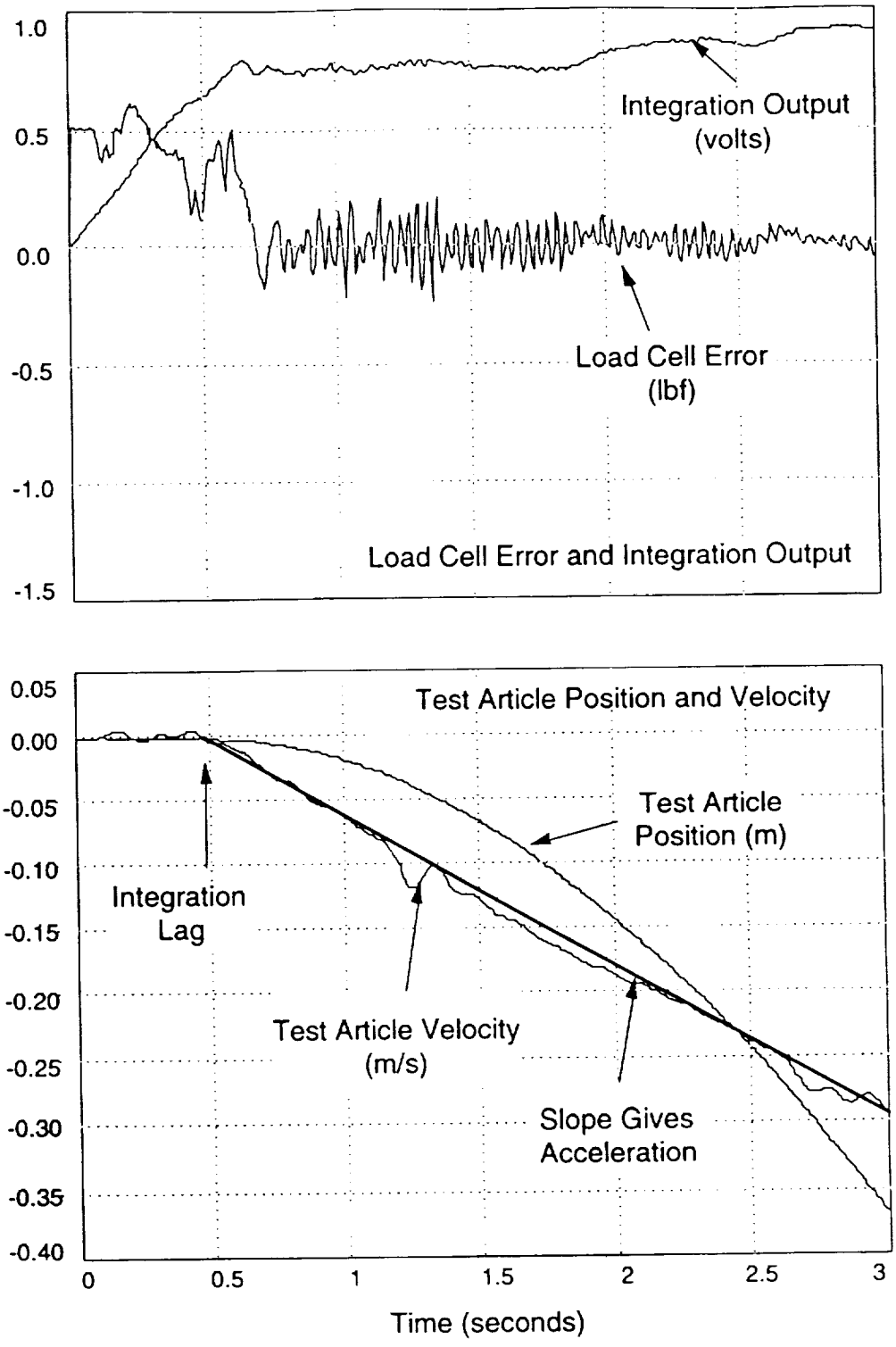

Figure 17. Typical rigid body response with integration gain

The major drawback of the integration gain can also be seen on Figure 17. Until the integration compensates for the passive friction, the test article experiences an

acceleration which is inconsistent with the force being applied. In Figure 17, during the period from 0 to .50 seconds, the controller output is growing but the test article has a near zero velocity and is not accelerating. The time the test article takes to reach a constant acceleration will be called the "integration lag" in the presented data.

The lag can be reduced by raising the integration gain, but this make the system less stable. As an example, an oscillation in the load cell error can be seen in figure 17 from 0.75 to 3.0 seconds. This vibration is the result of an excited suspension mode near 27 Hz, which eventually damps out. If the integration gain is increased, the magnitude of the oscillations increase and at a certain point becomes unstable. The relative stability achieved with various gains can be determined by monitoring the peak value of the load cell error due to this oscillation.

Test article velocity data was derived by differentiating the encoder position data. Because noise increases when differentiating a digital signal, the position data was prefiltered by a low pass filter, with a 20 Hz cut-off frequency before differentiation. From this data an approximation to the test article mean acceleration was calculated from the slope of a least squares straight line fit of the velocity. As figure 17 shows, the relatively constant slope in the velocity data indicates a nearly constant acceleration, as expected.

Figure 18 shows the integration lag time, maximum load cell error, and estimated acceleration error for a number of tests which used different values of integration gains. In one test a virtual force of -0.5 lbf was applied to the 38.9 lbm test article with dead band level set to 0.01 lbf. The other test used a real -0.65 lbf force applied to the same test article with identical dead band level. The acceleration error is expressed as the percent of deviation of the experimental acceleration from the theoretical acceleration. The time lag was calculated as a percentage of the theoretical test time, T, which is equal to:

$$T = \sqrt{\frac{2y}{a}}$$

where y is the vertical translation and a is the test article acceleration. The maximum load cell error, which provides quantification of the system's relative stability, is represented as a percentage of the test article weight.

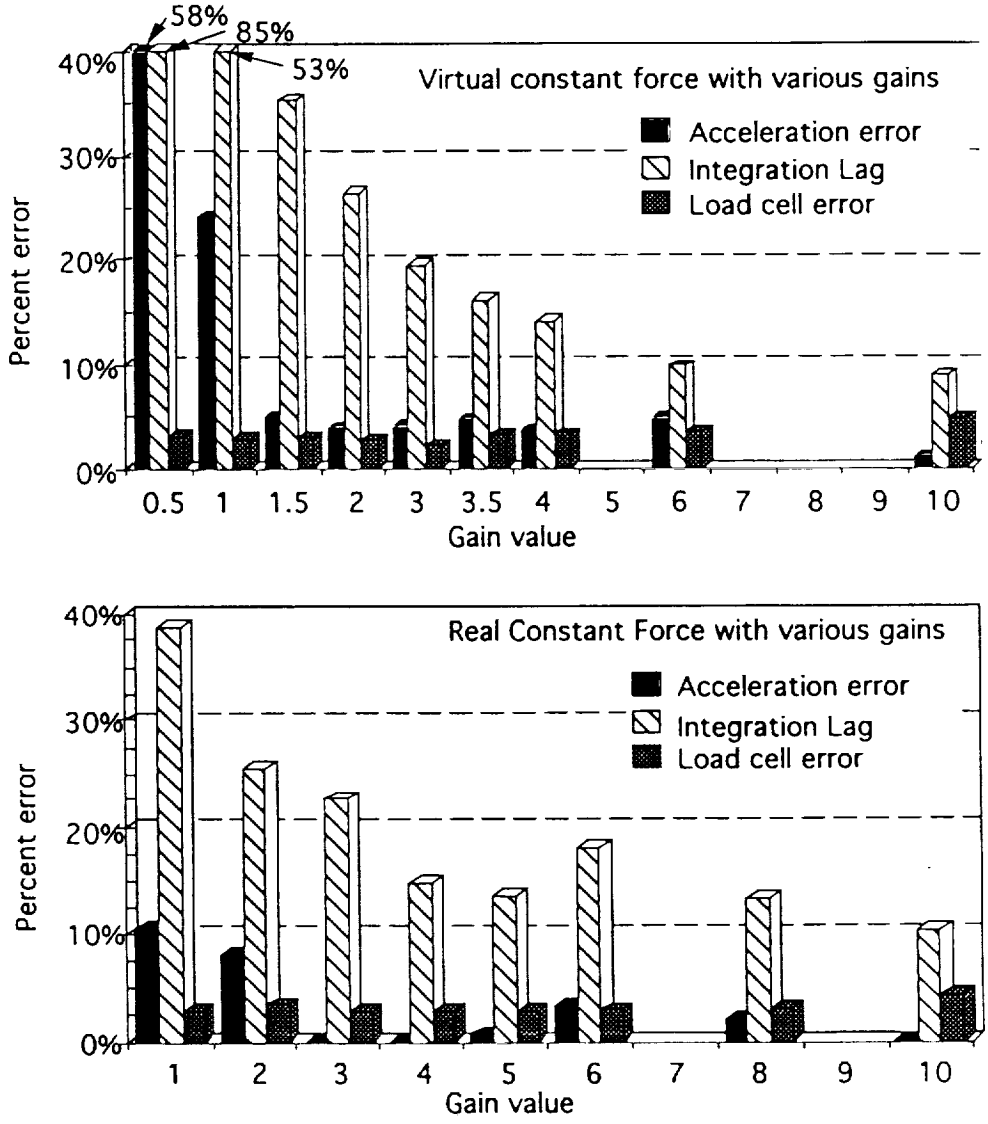

Figure 18. Response to various integration gains

Both tests indicate that with a gain above 2 volts/lbf the acceleration can be expected to be within 10% of the predicted value. The figure also show a tradeoff between the integration lag and the system instability. A small gain produces a large lag but a

relatively small load cell error. A large gain, in contrast, greatly reduces the lag time while producing a greater load cell error. A perfect suspension system would respond infinitely fast so no integration lag occurs no load cell error occurs. For convenience, tables listing the experimental values for the test are shown below.

Table 6. Variable gains test with a virtual input of -0.50 lbf

Integration Gain	Delay (sec)	Acceleration (m/sec)	Load Cell Error (lbf)
Theoretical	None	-0.13	None
0.5	2.40	-0.05	1.20
1.0	1.50	-0.01	1.10
1.5	1.00	-0.12	1.14
2.0	0.75	-0.12	1.00
3.0	0.55	-0.12	0.86
3.5	0.46	-0.12	1.23
4.0	0.40	-0.12	1.30
6.0	0.28	-0.12	1.32
10.0	0.25	-0.13	1.86

Table 7. Variable gains test with a real input of -0.65 lbf

Integration Gain	Delay (sec)	Acceleration (m/sec)	Load Cell Error (lbf)
Theoretical	None	-0.16	None
1	0.95	-0.15	1.08
2	0.63	-0.15	1.32
3	0.55	-0.16	1.13
4	0.36	-0.16	1.12
5	0.33	-0.16	1.06
6	0.44	-0.17	1.16
8	0.32	-0.17	1.22
10	0.25	-0.16	1.65

The results show that an integral controller will not eliminate lag or system instability. An improved controller might utilize proportional and derivative as well to help solve the problems. By themselves the proportional and derivative gain are not effective, nevertheless they may be valuable when used in conjunction with integral gain. For instance, the proportional gain may be able to speed the controller response to step inputs by giving extra gain while the integration error builds up, and the derivative gain may provide similar assistance for impulse forces. Future work aimed at a full PID

controller or perhaps some other controller scheme could provide a truly optimized response.

Integration Drift

Because of slight fluctuations in the load cell signal, noise during signal transmission, and slight fluctuations in the analog to digital conversion of a signal, a small bit of error exists in the signal from the load cell. Although this error is random, it tends to have a bias which varies from test to test. Because the average error is not zero the integrator takes the small deviations and produces a output signal. Over a period of time the test article begins moving even though no force has been applied.

The dead band in the controller is used to eliminate the drift problem. Measurements of integration drift were taken with dead band set to 0.00, 0.01 and 0.02 lbf [Figure 19]. Without a dead band all of the system noise passes to the integrator and integration drift is very significant. The 0.01 lbf dead band allows a small amount of noise but greatly reduces the output drift. With a dead band of 0.02 lbf, the noise is almost completely filtered out producing a very small integration drift. Although a large dead band produces a small drift, other factors must be considered. The system will not respond to any force smaller than the dead band level, reducing the system sensitivity. The optimum dead band is the smallest level which reduces the integration level to an acceptable value for the experiment being conducted. While integration drift may be important during long deployments, it will not be a factor during short rigid body acceleration tests.

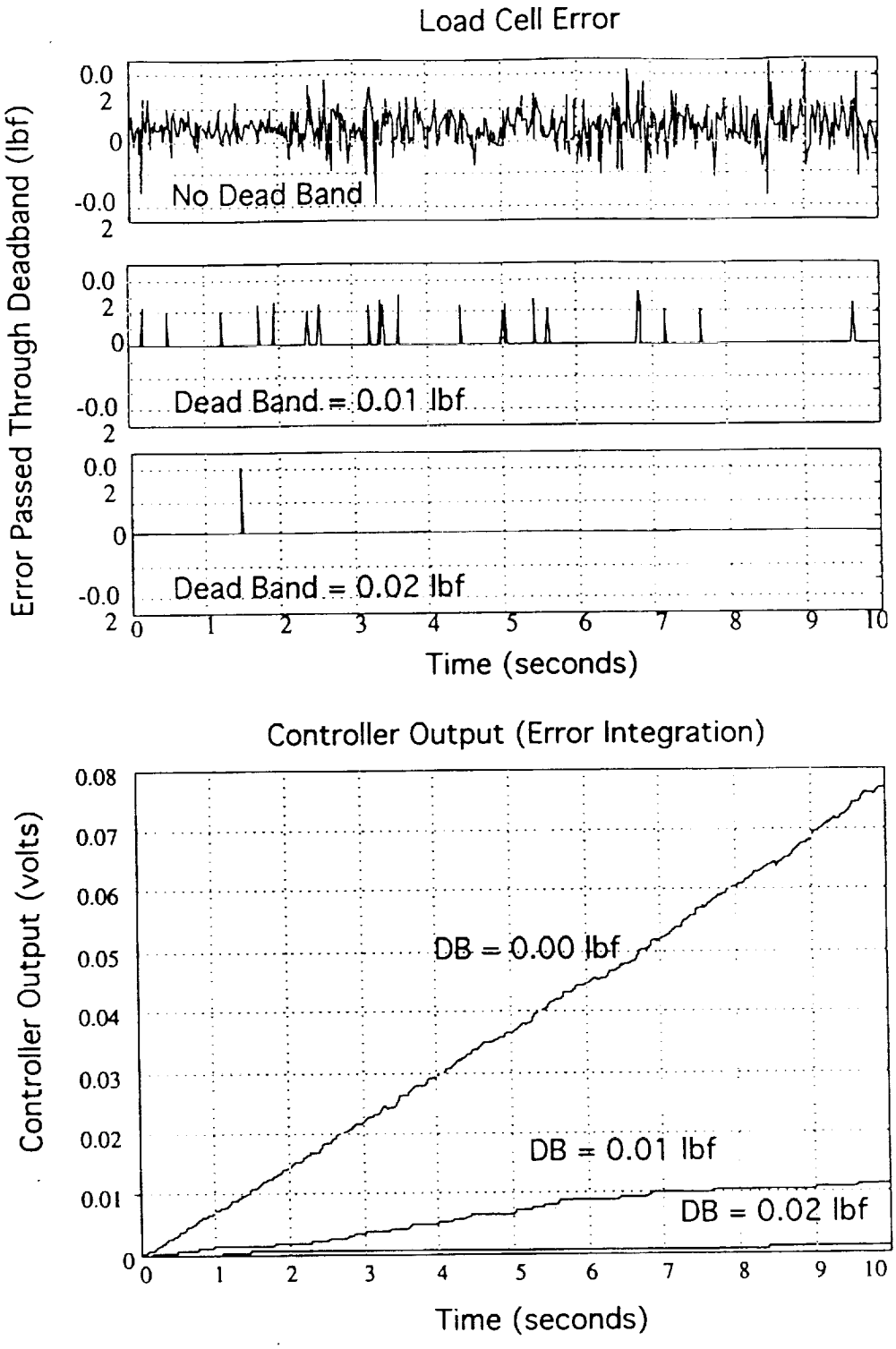

Figure 19. Effect of Dead Band on integration drift

3.4 Force Response Test

After determining how the system response changes with various control configurations, additional test were performed to quantify the systems ability to track different levels and types of forces.

For these tests the passive-plus-active system off-loaded the 38.9 lbm with a control dead band setting of 0.01 lbf. A constant real force was applied in varying magnitudes by placing different sized masses on the test article. The tests occur through a 0.504 meter region. After the test article translates that distance, the controller automatically shuts down and records the total test time. Values of load cell error, output voltage, and test article position were recorded at each for each pass through the control loop.

At each force level three controller configurations were used. The first, with the controller off, tests the passive system [Figure 20]. The other two tests used the active feedback with gains set to 4 and 10. Results for both gain level tests are shown in figure 21. The same normalized values used in figure 18 are shown here: the percent of acceleration error, time lag as a percent of total test time, and the maximum load cell error as a percent of test article weight.

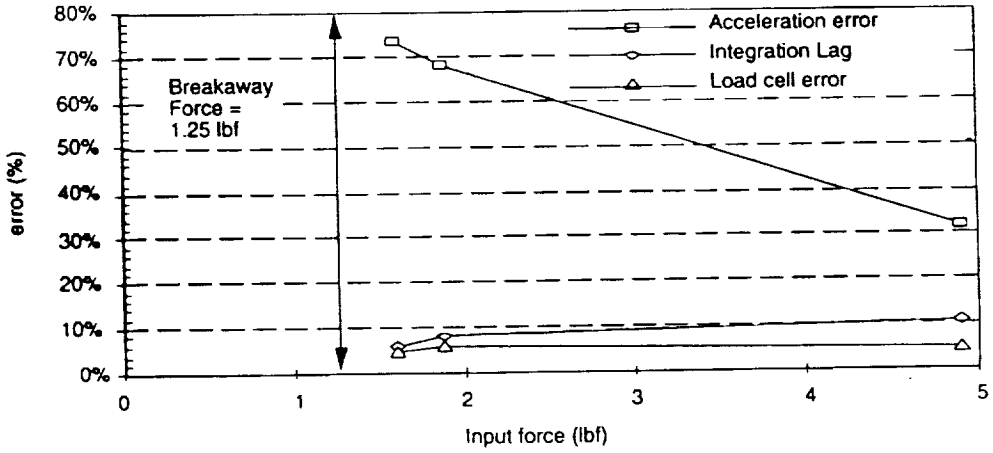

Figure 20. Passive-only response to various force levels

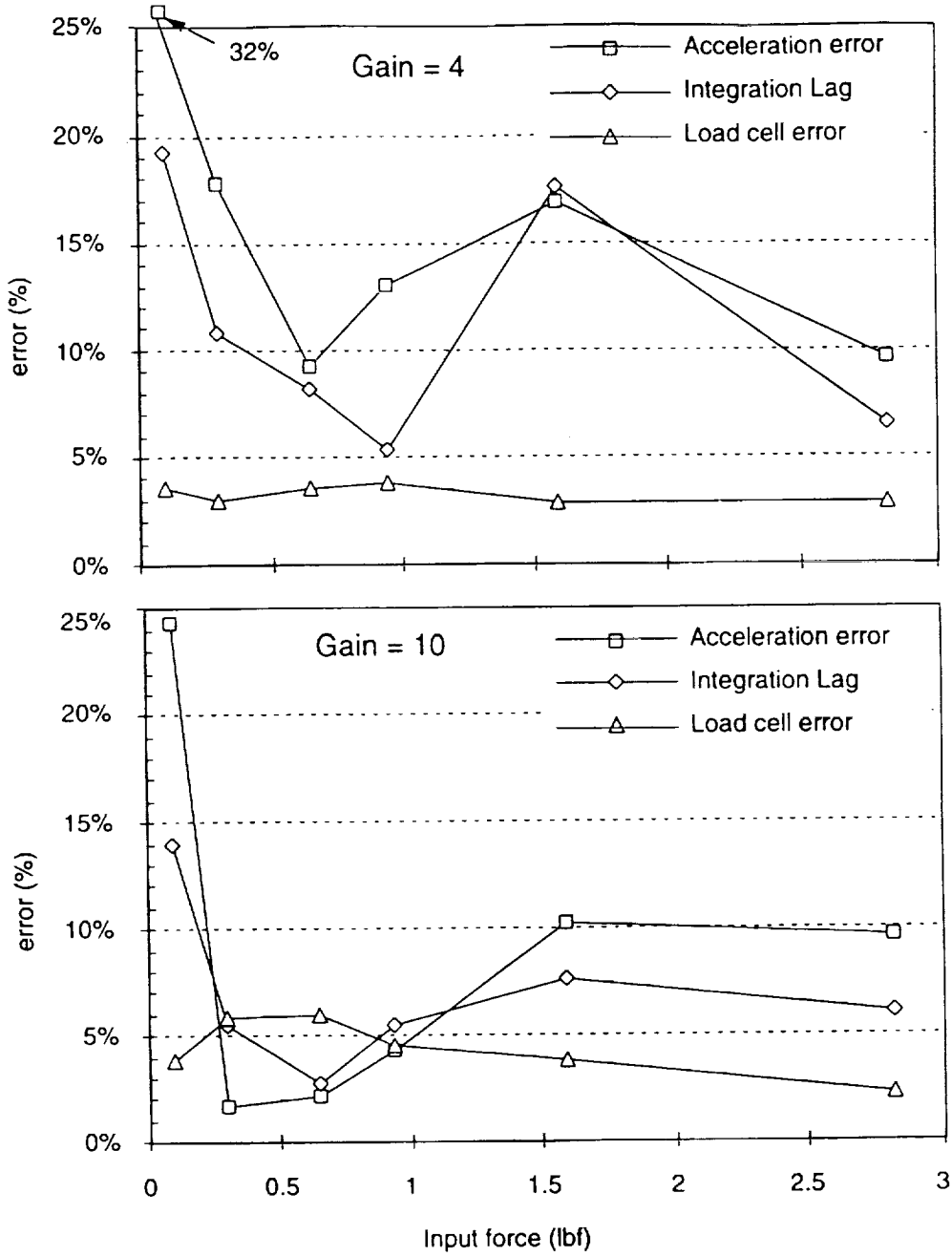

Figure 21. Passive-plus-active response to various force levels

Figure 20 reveals that the break away friction in the passive system is on the order of 1.25 lbf. An input force below this level produced no response from the system. Above this level the system responds with a high level of acceleration error. Without the active feedback to compensate, this is the level of response that can be expected.

The addition of the active feed back loop effectively offsets the friction and produces a much better response. Both levels of gain produce acceleration accurate to within 10% down to force levels near 0.25 lbf. A breakaway force level of approximately 0.1 lbf was found to exist. Between these force levels, 0.1 to 0.25 lbf the acceleration performance exceeds a 10% error level. A comparison of the results with different gains shows some tradeoff between reducing integration lag and keeping the load cell error small. For both tests, unfortunately, the level of integration lag remains between 5% and 10%.

Another factor not shown in these results is the presence of the suspension mode near 27 Hz. This vibration frequency occurred in the data from every test. The direct result to the rigid body tests is a small oscillation at 27 Hz superimposed on the constant acceleration. This mode can become very critical in experimentation with modes near this frequency and also in highly precise translational experiments such as deployment or multi-body docking.

4.0 MODAL ANALYSIS OF A SUSPENDED STRUCTURE

To determine the suspension system's effect on the vibrational characteristics of a suspended test structure, a modal survey was performed on a specially designed beam.

4.1 Test Article Selection

The 38.9 lbm highly flexible test article [Figure 22] was designed to have a relatively low first bending frequency near 10 Hz in one transverse direction. The other direction has much higher stiffness to elevate the frequencies, above 150 Hz, out of the bandwidth of the modal test. This eliminates any coupling between orthogonal modes and ensures that no out of plane modes appear in the frequency response function. The beam was also designed with a relatively short length to reduce sag in a one-g field. A simple MSC/NASTRAN model was used to estimate the first and second bending modes which were predicted to be at 7.6 Hz and 71 Hz.

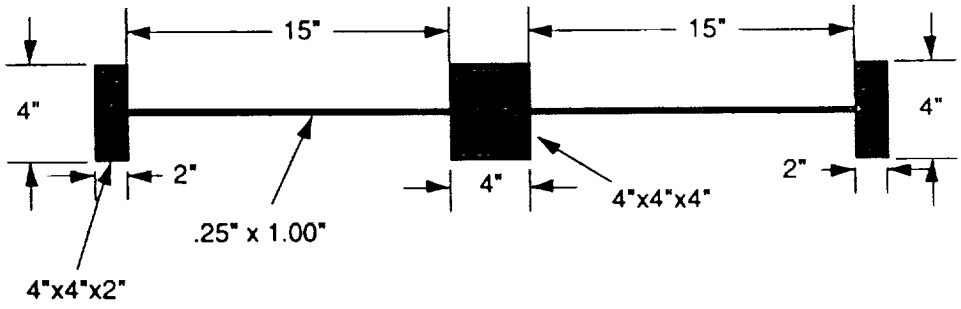

Figure 22. Highly flexible test article

4.2 Modal Survey of Highly Flexible Test Articles

Modal tests were performed with accelerometers on each of the concentrated masses parallel with the more flexible direction of the beam. An impulse was delivered to the center mass using a modal hammer . The accelerometers and input force were aligned

with the more flexible direction of the beam. Two modal tests were performed with the beam in different configurations. The first test was performed with the structure's flexible direction oriented with the horizontal plane and the structure suspended from a static cable. These results [Figure 23] closely represent the free-free modes of the structure because no external forces, including gravity, act in the horizontal direction. For the second test the flexible modes were oriented in the vertical direction with the structure suspended from the suspension system. The results are shown in the frequency response function [Figure 24], which gives the dB magnitude, phase, and coherence of the response.

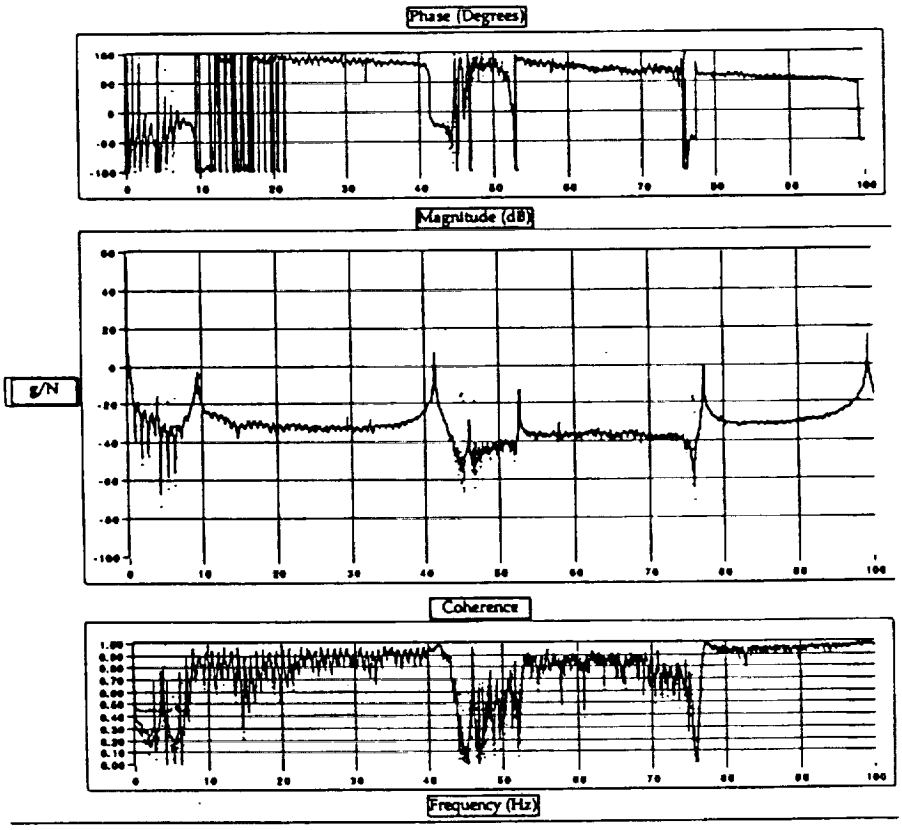

Figure 23. Horizontal modal test of flexible test structure

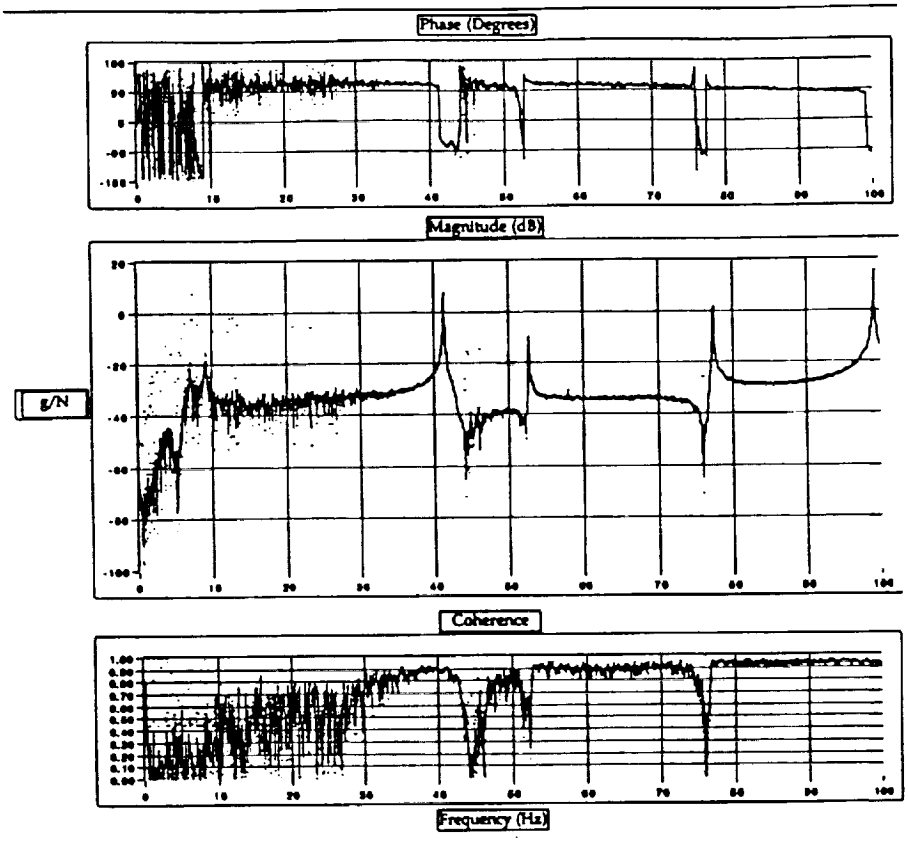

Figure 24. Modal test of suspended flexible test structure

For the experiment in the horizontal direction, the first and second bending modes appear at 9.2 Hz and 77 Hz. These compare closely to the predicted results from the finite element model. It should also be noted that three unpredicted peaks, near 41 Hz, 53 Hz, and 98 Hz also exist. These are probably either a cable pivot mode or some local modes in the beam which were not represented in the finite element model. Of more interest is an comparison of the modes from the actively suspended structure. It is apparent that the coherence and modal resolution are lost in the bandwidth of the suspension system controller, whose filter has a cut-off at 30 Hz. Instead of enhancing the response at these frequencies the modes appear highly damped. Above the

bandwidth of the controller, the frequency response is relatively unaffected. No shift in frequency appears and the peak amplitudes are almost identical

Table 8. Vibration frequencies of a highly flexible test article

	NASTRAN	Horizontal Test	Actively Suspended Test
First bending	7.6 Hz	9.2	9 (highly damped)
Second bending	71 Hz	77	77
Unidentified Modes	no match	41, 53, 98 Hz	41, 53, 98 Hz

For suspended structures with fundamental frequencies above this bandwidth experiments involving vibration measurements should produce accurate results. This includes structures like the baseline eight bay truss, with a fundamental frequency near 50 Hz.

5.0 EXTENSION TO A THREE DIMENSIONAL SYSTEM

The apparatus developed in the one DOF suspension system can also be used as part of a three dimensional suspension system which would maintain the vertical off-load of the test article weight within a three dimensional volume. This section describes a preliminary design concept and tests that were performed to validate portions of the concept.

In the three dimension suspension system concept, three cables are connected to a single point on the test structure. Each cable passes over a pulley located on the ceiling. These pulleys are laid out in an equilateral triangle. From the pulley each cable would attach to a modified version of the single DOF suspension system. This design, which forms and inverted tripod, minimizes the mass of the overall system, since the only moving parts are the cables and disks.

Instead of off-loading a constant force, as in the case of the one DOF system, the command tension in each cable must vary with test article position. The only constraint is that the vector sum of cable tensions has only a vertical component with magnitude equal to the weight of the structure. This will require changes in the off-load characteristics of the passive mechanism. Instead of providing constant force it will have to generate a force which varies with the position of the test article.

A central problem is the ability to use force feedback in this configuration. As mentioned above, the cable tension must vary with test article position. The means that the feedback scheme used for the one dimensional system will not directly work. In the one DOF system the most recent load cell reading in continuously compared against an initial reading to produce an error signal. For the three DOF system, the load cell

reading will change with test article position. The three DOF controller will have to compute the required cable tensions , based on test article position, and compare that to the cable tension measured with each load cell.

Equations were derived which determine cable tensions as a function of the length of each cable. The tension equations are derived from the free body diagram of a point mass with three cable forces balanced against the weight of the mass [Figure 25]. These equations produce a single valued relation between the cable lengths, $\overline{DA}, \overline{DB}$, and $\overline{DC}$, and the cable tensions, T_{DA}, T_{DB}, and T_{DC}.

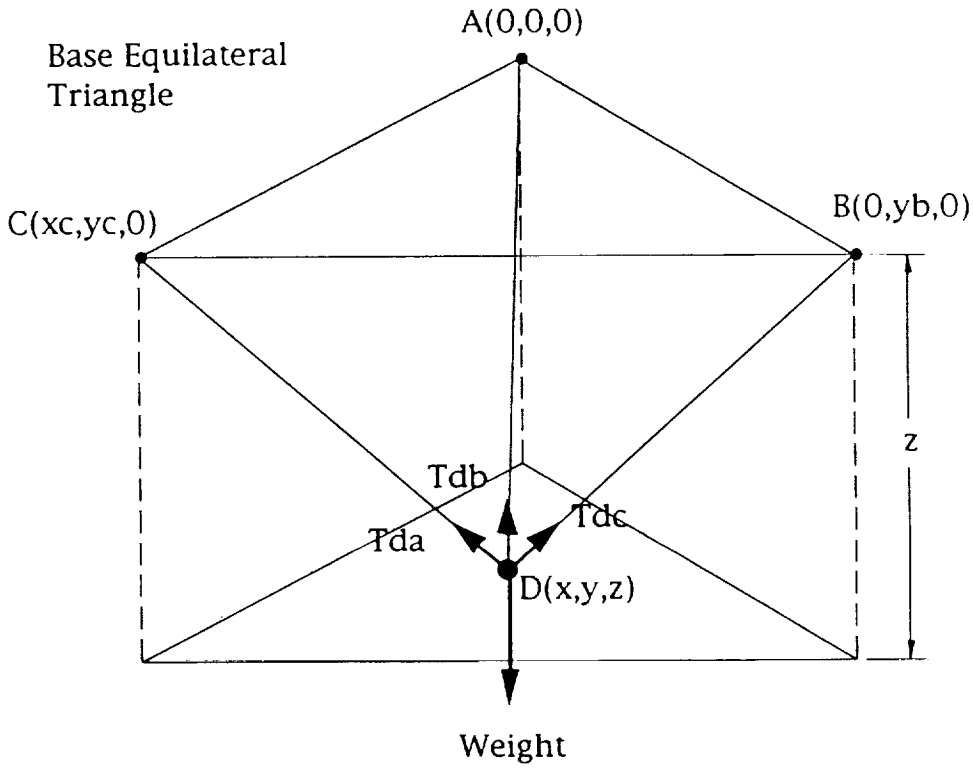

Figure 25. Tripod configuration for three DOF system

$$y_B = y_0 \qquad y_c = \frac{y_0}{2} \qquad x_C = \frac{\sqrt{3}y_0}{2}$$

$$T_{DA} = \frac{\overline{DA} \cdot W\left(\sqrt{3}y_0 - \sqrt{3}y - x\right)}{\sqrt{3}y_0 \cdot z}$$

$$T_{DB} = \frac{\overline{DB} \cdot W\left(\sqrt{3}y - x\right)}{\sqrt{3}y_0 \cdot z}$$

$$T_{DC} = \frac{2 \cdot \overline{DC} \cdot W \cdot x}{\sqrt{3}y_0 \cdot z}$$

A theoretical controller would execute in the following order. Encoders, either on the motors or attached to the overhead pulleys, would be used to calculate the current length of each cable. From these lengths, the prescribed tension for each cable can be calculated using the above equations. Simultaneously, a load cell from each of the cables would be read to determine the actual forces. If no external forces are acting on the system, the calculated and measured tensions should match. If a force does act on the test article the measured tensions will show some deviations from the calculated values. This difference can then be used as the error signal in a hypothetical controller which then commands the motors at each vertex to respond with the appropriate torque to move the test article.

The most basic assumption necessary for the proposed controller to work is the ability to predict the cable tension from a measurement of cable length. Without an accurate prediction a comparison to the measured cable tensions is meaningless. To test the ability to predict the cable tensions using only cable length measurements a very rudimentary inverted tripod was built. The vertices of the tripod base were 14 feet apart and 18 feet from the floor. This provided a spherical test region approximately 1.5 meters in diameter. A 50 lbm test article was used during testing [Figure 26]. Each of the three cables were attached to an eyebolt on the lumped mass. The cables passed over pulleys at each of the vertices and were attached to hand cranks which allowed manual positioning of the test article. Load cells identical to the one used in the single DOF system were used.

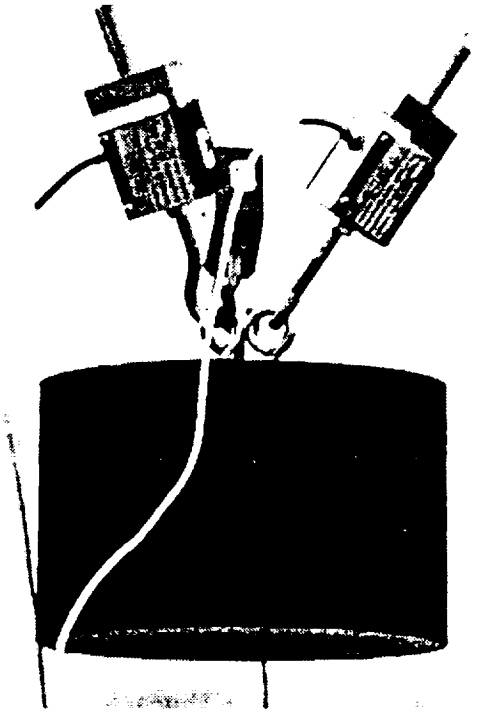

Figure 26. Photo of three DOF configuration test article

While calculating the cable tension may seem trivial on paper, many small errors can overwhelm the computation. The equations for cable tensions, show a proportional relation between any error in measuring the cable length or test article weight directly and the error in the calculated tension. Other errors result from inaccuracies in the geometry of the inverted tripod. Because a pulley is necessary for the cable to move smoothly, the exact position is not known. Furthermore, as the test article moves horizontally, at least one pulley must pivot. Vertical test article motions change the angle at which the cable leaves the pulley. These small deviations change the shape of the tripod. Also, in this configuration, the cables do not meet at a single point on the structure, an assumption used in formulating the equations. Cable stretch can also be a factor for cables of this length.

A test was performed to determine the accuracy with which the cable tension could be calculated based on cable length. The test article was positioned at a number of

locations within the possible test sphere. To see if the error is dependent on test article height the positions were grouped in horizontal slices. At each point, cable length was measured and a calculated tension was determined. The length for each position was measured manually and is accurate to approximately 1.0 inches. Simultaneously, the load cell readings provided a measured tension for each cable.

Tests were conducted at horizontal slices 12.2, 10.2, 8.2, and 6.2 feet below the vertices of the tripod. The error for each cable, as a percent of the 50 lbm test article, is shown at each of the horizontal levels in figure 27. The average value of the error at all locations was 0.56 lbf.

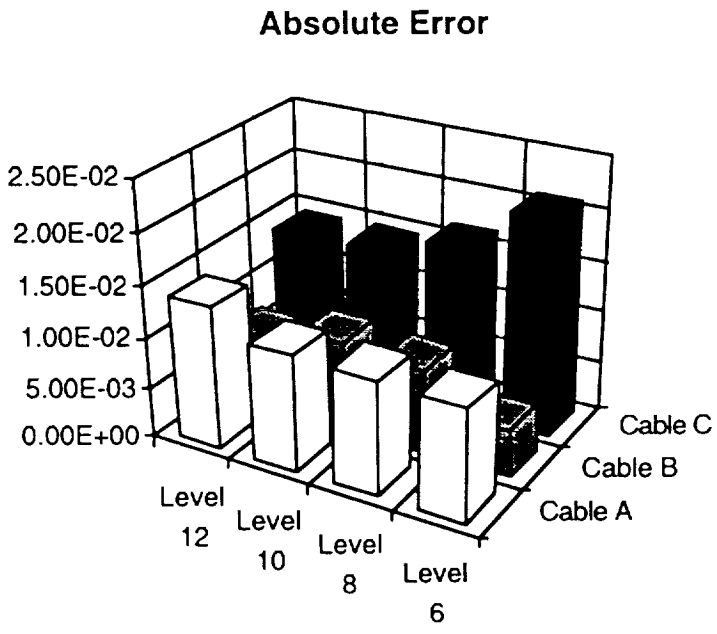

Figure 27. Error in cable tension test

Much of this error is a result of the methodology used to measure cable length. Future tests should include encoders to continuously monitor cable length. This should

greatly improve the 1.0 inch resolution currently available. The ability to accurately calculate cable tension is critical in producing a three DOF system.

6.0 CONCLUSIONS AND RECOMMENDATIONS

The primary goal of this research was to produce a first generation suspension system capable of off-loading test structures for use in space construction type experiments. One motivation was the production of a fully function system for one dimensional testing. But more importantly, this research identifies critical technology areas for further research for an improved single DOF system as well as a possible three dimensional configuration. Within these objectives, the conclusions are divided into two sections. The first focuses on the system's current ability to simulate the motion of an orbiting structure. The second looks at the problems which must be overcome to improve the system in the future.

6.1 Current Capabilities

Two major types of testing were performed with the one dimensional suspension system; rigid body acceleration and modal response of a suspended test article. Additionally, preliminary testing was done to examine the feasibility of the three dimensional system. A brief synopsis of these results follows

While the passive-only system has a friction level of 1.25 lbf, active force feedback compensation is able to reduce this by an order of magnitude to 0.1 lbf. Simulations involving rigid body accelerations can be expected to be within 10% of the values achieved on orbit. The best performance was achieved using integral only feedback with a dead band of 0.01 lbf.

Integration lag was a major problem that was identified with the controller. The lag can be reduced by raising the control gain. Increasing this gain tends destabilizes the 27

Hz suspension mode. These two factors must be considered during controller configuration and result in some limitations of the suspension system. The lag prohibits effective off-loading in experiments involving rapidly changing inputs. Nevertheless, the system can be useful in vertical deployment experiments and also vertical rigid body translation tests.

The results of the modal survey suggest that any attempt to examine test structure frequencies within the bandwidth of the controller will produce a highly damped response. For tests which involve structures with higher frequency modes, the results are within a few percent of the measured unrestrained values.

For an inverted tripod three dimensional suspension system the cable tensions can be predicted based on cable length. The accuracy of this prediction is important to the ability to utilize a force feedback control design. Current tests with static cables demonstrate an ability to predicted cable tension to within 0.5 lbf. This accuracy will have to be substantially improved before a three dimensional control concept can be implemented further.

6.2 Recommendations for Future Systems

The three most critical problems identified in the currently implemented system are the integration lag, the passive sub-system friction, and the presence of the 27 Hz suspension mode. Refinements in the controller and the passive system could reduce or eliminate these problems. Suggestions for improvements in these areas follow.

Further testing of the system should be performed to better identify its vibration characteristics. A frequency response function of the suspension system could be performed by putting a sine dwell force into a lumped mass test structure suspended from the suspension system and measuring the resulting acceleration. This would

identify system modes and might help locate the source of the 27 Hz mode which was so pervasive during testing. Suggestions for reduce the effect of this mode could include eliminating it mechanically, if possible, or utilizing a stop band filter for the controller

The current controller is limited to an execution frequency of 150 Hz primarily by limitations in the LabVIEW software. With new software upgrades or direct programming of the code in a language like C the frequency can probably be raised to near 1000 Hz. Raising the sampling frequency of the controller would also allow the anti-aliasing filter cutoff to be raised to somewhere around 200 Hz. This would allow tests which examine changes in rigid body acceleration for various controller speeds and filter cut-off frequencies. The modal test should also be repeated to determine if the structures modes within an expanded controller bandwidth are still highly damped.

Further controller improvements include optimizing the PID gains. As mentioned earlier the optimum controller will probably use full PID control and not just integration feedback. The primary goal of these refinements should be reducing the integration lag toward zero. This task will be easier if the problem involving the 27 Hz suspension mode can be solved. The integration gain has been limited to about 15 volts/lbf because any higher gains drive the 27 Hz mode to instability. With this mode removed or filtered out, the integration can probably be raised significantly without destabilizing the system. This would result in a dramatic reduction in the lag time. Future tests should also directly measure the mass and stiffness that the suspension system adds to the test article.

Reducing the friction throughout the system should also greatly improve system performance. Less friction would reduce the breakaway force needed and consequently reduce integration lag. A full study could be conducted to determine the various sources of friction and methods to reduce it. The friction sources include the overhead pulleys,

the bearings used in the cable guide, the bearings in the disk support shaft, spring and mandrel binding, and the servo motor and encoder.

Moving the cable guide further from the disk will reduce friction generated in the cable guide bearings. It is even possible to remove the cable guide and let a pulley affixed to the ceiling act in its place. Difficulties with this include the inability to relocate the device to a facility with different ceiling height. It also eliminates the modularity of the passive system. Mounting the system in an inverted position from the ceiling will remove the necessity of the two overhead pulleys, eliminating their friction. Friction from the shaft bearings is probably the least significant friction source but reductions may be possible.

The greatest amount of friction is probably from the torsional spring. The friction seems to increases as the spring is deflected, when the coils contact each other and when binding on the mandrels becomes significant. To verify this, tests of the systems breakaway friction should be performed at positions with large and small spring deflections. Different mandrel designs may be able to reduce the contact friction. A spring utilizing more coil spacing or even a design with helical spiral coils might prevent adjacent coils from coming in contact with each other. Final refinements could include upgrades to a motor and encoder with less friction.

Overall, this research has proven the concept of a passive constant force mechanism augmented by an active force feedback controller is effective in off-loading the weight of a test article over large regions. Active control reduced the effect of break-away friction by an order of magnitude, and future system should be able to improve on this performance.

REFERENCES

[1] Quartararo, R., Dr. Hasselman, T.K., "Microgravity Suspension of Flexible Space Structures," Phillips Laboratory Final Report, November, 1991, PL-TR--91-3071.

[2] Kienholz, D.A., "A Pneumatic/Electric Suspension System for Simulating On-Orbit Conditions," Presented at the Winter Annual Meeting of the American Society of Mechanical Engineers, Dallas, Nov. 25-30, 1990, 90-WA/Aero-8.

[3] Cooley, V.M. and Giunta, A. A., "Laboratory Evaluation of Two Advanced Suspension Devices for Ground Vibration Testing of Large Space Structures," *Proceedings of the 33th AIAA/ASME/ASCE/AHS/ASC Structures, Structural Dynamics and Materials Conference*, 1992, AIAA-92-2334-CP

[4] Woodard, S. E. and Housner, J. M., "Nonlinear Behavior of a Passive Zero-Spring-Rate Suspension System." J. Guidance Vol. 14, No. 1. Jan.-Feb. 1991, pp. 88-89.

[5] Hasselman, T. K., Editor, "AIAA/AFOSR Workshop on Microgravity Simulation in Ground Validation Testing of Large Space Structures, Final Report," EMA-TR-90-1153.

[6] Yang L. F., Chew M. and Juang J. N., "Ground-Based Testing of the Dynamics of Flexible Space Structures Using Band Mechanisms," Doctoral dissertation of first author, Old Dominion University, Norfolk.

[7] Nicholas P. C., *Mechanisms and Mechanical Devices Sourcebook*. New York: McGraw-Hill, Inc., 1991.

[8] Honeybee Robotics, "A Gravity Compensation System for Simulation of On-Orbit Telerobotic Operations," Final Report, New York, June 28, 1991, SBIR 90-1.

[9] Spring Manufacturers Institute, Inc., *Newcomb Spring Corp., Spring Design Manual," 1991.*

[10] Xylon, Nordic Ware, Commercial Coatings Division. Minneapolis, MN

[11] LabVIEW 2 Users Manual, National Instruments Corporation, September 1991 Edition, Austin, TX.